Journal of Power Sources 240 (2013) 18–25

Contents lists available at SciVerse ScienceDirect

Journal of Power Sources

journal homepage: www.elsevier.com/locate/jpowsour

Lithium ion transport properties of high conductive tellurium substituted $Li_7La_3Zr_2O_{12}$ cubic lithium garnets

C. Deviannapoorani, L. Dhivya, S. Ramakumar, Ramaswamy Murugan*

Department of Physics, Pondicherry University, Puducherry 605 014, India

HIGHLIGHTS

- Fast Li^+ conductive lithium garnets were obtained by Te substitution in $Li_7La_3Zr_2O_{12}$.
- Cubic phase is successfully obtained at lower sintering temperature around 750 °C.
- $Li_{6.5}La_3Zr_{1.75}Te_{0.25}O_{12}$ exhibits a maximum Li^+ conductivity of 1.02×10^{-3} S cm^{-1} at 30 °C.

ARTICLE INFO

Article history:
Received 4 February 2013
Received in revised form
14 March 2013
Accepted 19 March 2013
Available online 6 April 2013

Keywords:
Solid electrolytes
Lithium garnets
Ionic conductivity
Lithium ion battery

ABSTRACT

In this paper synthesis, structure and Li^+ transport process of $Li_{7-2x}La_3Zr_{2-x}Te_xO_{12}$ ($x = 0.125$ and 0.25) lithium garnets are reported. Preparation of high Li^+ conductive $Li_7La_3Zr_2O_{12}$ (LLZ) in cubic phase by conventional solid state method demands sintering it around 1200 °C for 36 h in Al_2O_3 crucible. Cubic phase lithium garnet is successfully obtained at lower sintering temperature around 750 °C with the substitution of Zr^{4+} by Te^{6+} in the garnet lattice over the investigated composition range. Among the investigated compounds $Li_{6.5}La_3Zr_{1.75}Te_{0.25}O_{12}$ sintered at 1100 °C exhibits a maximum room temperature total (bulk + grain boundary) ionic conductivity of 1.02×10^{-3} S cm^{-1}. The present studies reveal the stabilization of the cubic garnet phase relatively at lower sintering temperature along with an enhancement in Li^+ conductivity with lithium content lesser than 7 by suitable doping in $Li_7La_3Zr_2O_{12}$.

1. Introduction

Among the rechargeable batteries, lithium ion rechargeable batteries have been more widely used in portable electronic devices because they provide higher energy density and generate high voltage. Inorganic solid fast Lithium ion (Li^+) conductor based batteries are expected to overcome limitations over the safety concerns of currently available organic polymer electrolyte based lithium batteries. The main features required for a successful solid electrolyte are high Li^+ conductivity, negligible electronic conductivity and wide electrochemical window. In recent years, a series of garnet-like structural compounds have been investigated as a novel family of fast lithium ion conductors by Weppner and his group [1–10]. Among them, lithium garnet with nominal chemical formula $Li_7La_3Zr_2O_{12}$ (LLZ) reported by Murugan et al. has received considerable importance in recent times as result of its high total (bulk + grain boundary) ionic conductivity of 5×10^{-4} S cm^{-1} at 25 °C combined with good chemical stability against potential electrodes and stability against lithium metal [5].

LLZ in tetragonal phase exhibits two orders of lower conductivity compared to their cubic phase [11]. Disordered arrangement of Li^+ across tetrahedral and octahedral sites is the prime factor for the observed high conductivity in cubic lithium garnet. In contrast complete ordering of Li^+ across all of octahedral and one third of tetrahedral leads to lower ionic conductivity in the tetragonally distorted LLZ compared to cubic phase. Studies also suggested that the unintentional incorporation of Al^{3+} ions into LLZ during the high-temperature solid state synthesis using alumina crucibles helps to stabilize the cubic phase against the tetragonal one [12–15]. Following initial results of high Li^+ conduction in the LLZ there has been significant interest in the synthesis, structural and electrical conductivity of Ta, Nb, Al, Ga, Si, Y substituted cubic phase LLZ [16–24].

For further understanding of the Li^+ dynamics in lithium garnets and the effect of Tellurium (Te) substitution on structure and Li^+ transport properties of LLZ a systematic investigations has been carried out in the present work on $Li_{7-2x}La_3Zr_{2-x}Te_xO_{12}$ ($x = 0.125$ and 0.25) lithium garnets.

* Corresponding author.
E-mail address: moranamurugan@pec.edu (R. Murugan).

0378-7753/$ – see front matter © 2013 Elsevier B.V. All rights reserved.
http://dx.doi.org/10.1016/j.jpowsour.2013.03.166

2. Experimental

Lithium garnets with nominal compositions $Li_{7-2x}La_3Zr_{2-x}Te_xO_{12}$ with $x = 0.125$ i.e., $Li_{6.75}La_3Zr_{1.875}Te_{0.125}O_{12}$ and $Li_{7-2x}La_3Zr_{2-x}Te_xO_{12}$ with $x = 0.25$ i.e., $Li_{6.5}La_3Zr_{1.75}Te_{0.25}O_{12}$ were prepared from the stoichiometric amount of $LiOH.H_2O$ (Sigma–Aldrich, >99%; 15 wt.% excess was added to compensate the loss of lithium during sintering at high temperature), La_2O_3 (Merck, >99% pre dried at 900 °C for 24 h), ZrO_2 (Acros, 98%) and TeO_2 (Himedia, 97%) by conventional solid state method. The powders were ball milled using Zirconia balls in 2-propanol for 6 h using a Pulverisette7, Fritsch. After the evaporation of solvents, the powders were heated at 750 °C for 6 h and then cooled down to room temperature. The obtained powders were ground again for another 6 h using zirconia balls in 2-propanol. After the evaporation of the solvents the powders were pressed into pellets under isostatic pressure. The pellets were covered with the same mother powder to reduce possible lithium loss and heated in a closed alumina crucible from room temperature to 1100 °C and held at this temperature for 15 h.

The sintered pellets were ground into powder and were characterized by Powder X-ray diffraction (PXRD) (X'pert PRO PANalytical) with Cu-K_α radiation of $\lambda = 1.5418$ Å at room temperature in 2θ range from 10 to 80° with a step of 0.025° to confirm the phase formation. The surface morphology of the sintered pellets was characterized by scanning electron microscope (SEM; HITACH S-3400N).

The electrical conductivity measurements were performed on the prepared pellets using Li-ion blocking Au-electrodes (cured at 600 °C for 1 h) in the temperature range from −100 to 100 °C using a Novocontrol Concept 80 broadband dielectric spectrometer (BDS).

3. Results and discussion

3.1. Powder X-ray diffraction (PXRD)

Fig. 1 shows the Powder X-ray diffraction (PXRD) pattern of $Li_{6.75}La_3Zr_{1.875}Te_{0.125}O_{12}$ and $Li_{6.5}La_3Zr_{1.75}Te_{0.25}O_{12}$ sintered at 750 °C along with the reported pattern of cubic LLZ [5]. The measured PXRD patterns as shown in Fig. 1 exhibit cubic phase and do not indicate any additional diffraction lines corresponding to tetragonal symmetry. The PXRD pattern shown in Fig. 1 exhibits additional weak reflection corresponding to minor impurity phase $ZrO_{1.96}$ in the case of $Li_{6.75}La_3Zr_{1.875}Te_{0.125}O_{12}$ and La_2O_3 as a minor phases in the case of $Li_{6.5}La_3Zr_{1.75}Te_{0.25}O_{12}$.

Fig. 2 shows the Powder X-ray diffraction (PXRD) patterns of $Li_{6.75}La_3Zr_{1.875}Te_{0.125}O_{12}$ and $Li_{6.5}La_3Zr_{1.75}Te_{0.25}O_{12}$ sintered at 1100 °C along with the reported pattern of cubic LLZ [5]. $Li_{6.75}La_3Zr_{1.875}Te_{0.125}O_{12}$ exhibits cubic phase with minor secondary phase of Li_2ZrO_3. The PXRD pattern for $Li_{6.5}La_3Zr_{1.75}Te_{0.25}O_{12}$ confirms the garnet like structure with cubic symmetry without indicating any additional peaks corresponding to any impurity phases. Compound with the chemical formula $Li_{6.75}La_3Zr_{1.875}Te_{0.125}O_{12}$ and $Li_{6.5}La_3Zr_{1.75}Te_{0.25}O_{12}$ were found to be crystallized in cubic phase with the lattice constant $a = 12.9469$ Å and $a = 12.9134$ Å, respectively. The substitution of smaller Te^{6+} (ionic radius, $r = 0.56$ Å in VI coordination) for the larger Zr^{4+} (ionic radius, $r = 0.72$ Å in VI coordination) together with the simultaneous decrease of the lithium content leads to decrease of the lattice parameter with increasing x in $Li_{7-2x}La_3Zr_{2-x}Te_xO_{12}$ [25]. The serious problems in the preparation of LLZ in cubic phase by solid state method is that sintering the sample at high temperature around 1200 °C for 36 h in Al_2O_3 crucible and intermittent grinding are essential [5]. The present PXRD results indicate that the cubic phase was successfully achieved relatively at lower sintering temperature around 750 °C with the substitution of Zr^{4+} by Te^{6+} in the garnet lattice over the investigated composition range.

3.2. Microstructural analysis

The SEM images of surfaces of the $Li_{6.75}La_3Zr_{1.875}Te_{0.125}O_{12}$ and $Li_{6.5}La_3Zr_{1.75}Te_{0.25}O_{12}$ pellets sintered at 1100 °C are shown in Fig. 3(a) and (b), respectively. The $Li_{6.5}La_3Zr_{1.75}Te_{0.25}O_{12}$ pellet exhibits high densification and grains were in good contact with each other compared to $Li_{6.75}La_3Zr_{1.875}Te_{0.125}O_{12}$. A glass like phase covering over the grains was observed in the SEM image of $Li_{6.5}La_3Zr_{1.75}Te_{0.25}O_{12}$. Energy dispersive analysis by X-ray (EDAX) indicated the incorporation of Al^+ from the Al_2O_3 crucible during sintering process as 1.85 and 2.95 wt.% in $Li_{6.75}La_3Zr_{1.875}Te_{0.125}O_{12}$

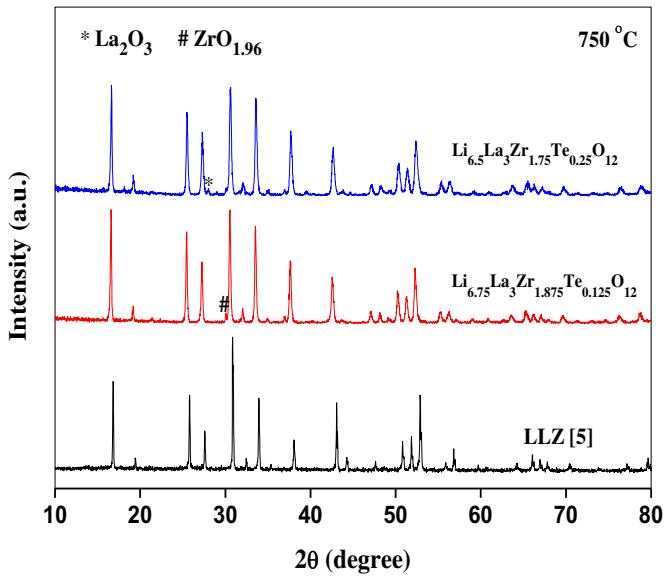

Fig. 1. PXRD patterns for the composition $Li_{6.75}La_3Zr_{1.875}Te_{0.125}O_{12}$ and $Li_{6.5}La_3Zr_{1.75}Te_{0.25}O_{12}$ sintered at 750 °C with standard pattern of cubic LLZ [5].

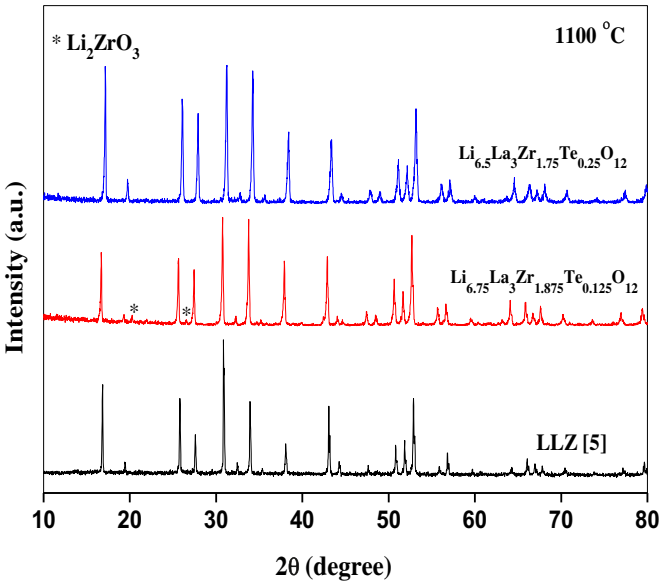

Fig. 2. PXRD patterns for the composition $Li_{6.75}La_3Zr_{1.875}Te_{0.125}O_{12}$ and $Li_{6.5}La_3Zr_{1.75}Te_{0.25}O_{12}$ sintered at 1100 °C with standard pattern of cubic LLZ [5].

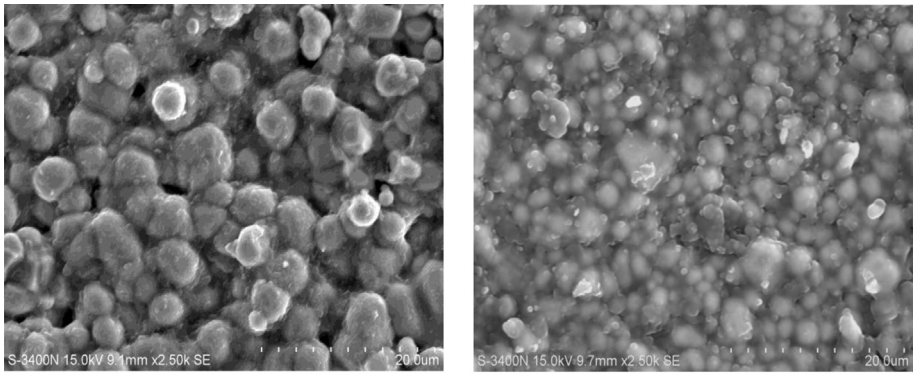

Fig. 3. SEM images of (a) $Li_{6.75}La_3Zr_{1.875}Te_{0.125}O_{12}$ and (b) $Li_{6.5}La_3Zr_{1.75}Te_{0.25}O_{12}$ pellets sintered at 1100 °C.

and $Li_{6.5}La_3Zr_{1.75}Te_{0.25}O_{12}$, respectively. Although the EDAX analysis indicated the incorporation of Al^{+}, further detailed neutron diffraction and ^{27}Al magic angle nuclear magnetic resonance (MAS NMR) are essential to understand the kind of Al^{+} distribution on the different sites of crystal lattice and transmission electron microscopy (TEM) studies for identification of kind of Al^{+} incorporated phase at the grain boundary and its role in the ionic conductivity of the investigated samples.

3.3. Electrical properties

3.3.1. Impedance analysis

In order to understand the effect of Te substitution in LLZ on the ionic conductivity systematic impedance measurements was performed on the prepared pellets in the temperature interval from −100 to 100 °C. The impedance plots (Cole–Cole) measured at −50, 0 and 30 °C for the composition of $Li_{6.75}La_3Zr_{1.875}Te_{0.125}O_{12}$ and $Li_{6.5}La_3Zr_{1.75}Te_{0.25}O_{12}$ sintered at 1100 °C are shown as Fig. 4(a) and (b), respectively. The high frequency portion of the impedance plot (for temperature 0 and 30 °C) is zoomed for clarity and given as inset in Fig. 4(a) and (b). The appearance of a capacitive tail for all the investigated samples at the low frequency side in the case of the applied ionically blocking Au electrode as shown in Fig. 4(a) and (b) is an indication that the investigated material is ionically conducting in nature. The lack of clear two semicircles in the higher frequency part of the impedance plots in Fig. 4(a) and (b) indicates that the bulk and grain boundary resistance could not be well resolved. We have considered uniformly the total (bulk + grain boundary) ionic conductivity for the presentation of conductivity results over the investigated temperature range.

Arrhenius plot for total ionic conductivity of $Li_{6.75}La_3Zr_{1.875}Te_{0.125}O_{12}$ and $Li_{6.5}La_3Zr_{1.75}Te_{0.25}O_{12}$ samples sintered at 1100 °C shown in Fig. 5 indicates that there is no appreciable shift in the conductivity and this implies that the investigated samples are thermally stable without any phase transition in the measured temperature range from −100 to 100 °C.

The temperature dependence of the conductivity can be expressed by the Arrhenius Eq.,

$$\sigma T = A\exp\left(\frac{-E_a}{k_B T}\right) \quad (1)$$

where A is the pre-exponential parameter, k_B is Boltzmann's constant and T is the absolute temperature. The activation energies (E_a) were estimated from the slope of the log σT versus 1000/T. The activation energies obtained for total conductivity of $Li_{6.5}La_3Zr_{1.75}Te_{0.25}O_{12}$ in the temperature range from room temperature to 100 °C is 0.37 eV, which is comparable to that of 0.31 eV (18–300 °C) of $Li_7La_3Zr_2O_{12}$ [5]. The total conductivity measured at various temperatures derived from the intercepts of high frequency

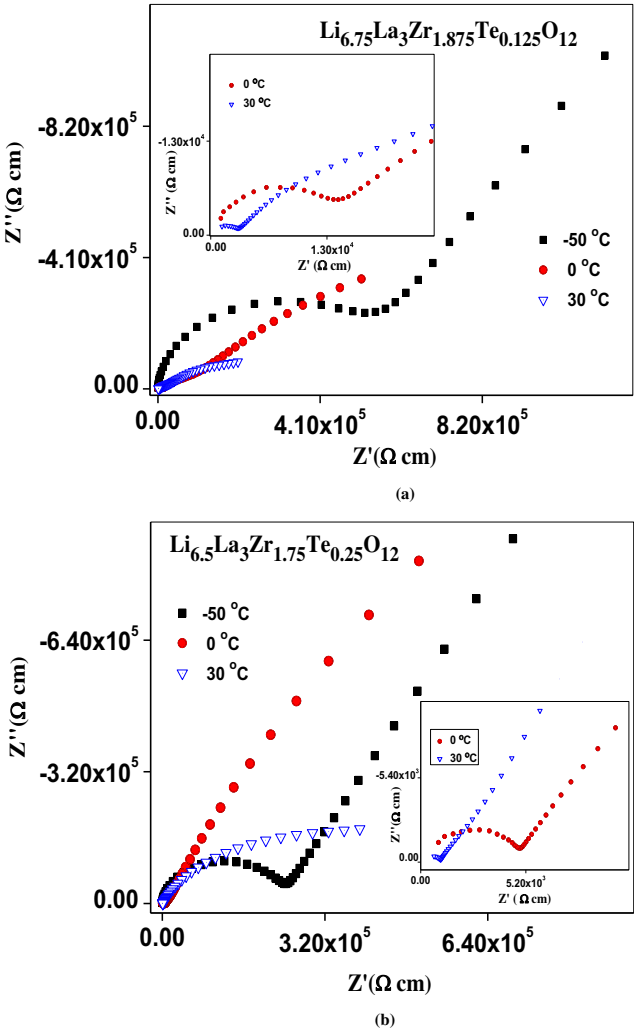

Fig. 4. AC impedance plot of (a) $Li_{6.75}La_3Zr_{1.875}Te_{0.125}O_{12}$ and (b) $Li_{6.5}La_3Zr_{1.75}Te_{0.25}O_{12}$ measured at −50 °C, 0 °C and 30 °C. The impedance plot in the high frequency region is shown as inset.

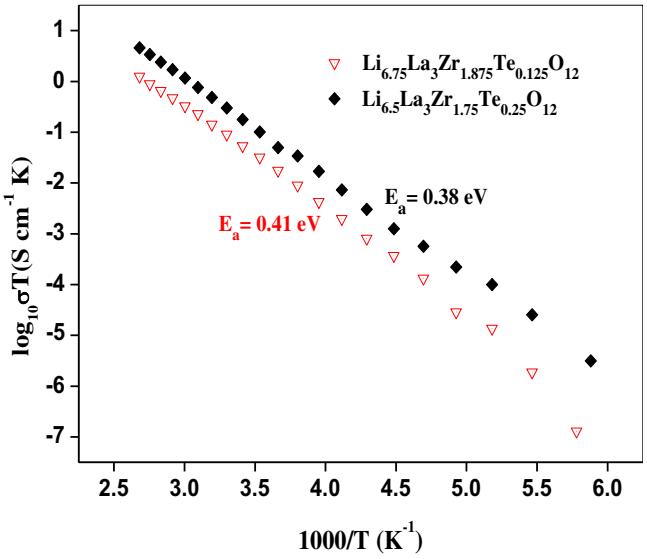

Fig. 5. Arrhenius plot for total lithium ion conductivity of $Li_{6.75}La_3Zr_{1.875}Te_{0.125}O_{12}$ and $Li_{6.5}La_3Zr_{1.75}Te_{0.25}O_{12}$ in the temperature interval from −100 to 100 °C.

semicircles with the real axis and activation energies derived from Arrhenius plot for total conductivity (in the temperature range from −100 to 100 °C) for the investigated samples sintered at 750 °C and 1100 °C are tabulated in Tables 1 and 2, respectively. The ionic conductivity for the samples sintered at 750 °C was found to be lower than that of the samples sintered at 1100 °C. Earlier investigations on ionic conductivity of cubic $Li_{7-x}La_3Zr_{2-x}Ta_xO_{12}$ and $Li_{7-x}La_3Hf_{2-x}Ta_xO_{12}$ indicated that the maximum conductivity for the composition around $x = 0.4 \pm 0.1$ [16,26,27]. In the present investigation the maximum room temperature (30 °C) total ionic conductivity of 1.02×10^{-3} S cm^{-1} was achieved for the composition $Li_{6.5}La_3Zr_{1.75}Te_{0.25}O_{12}$ sintered at 1100 °C.

3.3.2. *ac conductivity behavior*

The ac conductivity spectra of many solids, including glasses, polymers, crystals, and semiconductors, were found to obey the following Jonscher's universal power law [28],

$$\sigma\prime(\omega) = \sigma_{dc} + A\omega^n \tag{2}$$

where σ_{dc} is frequency-independent conductivity, A is pre-factor that depends on temperature and composition and it is defined as $A = (\sigma_{dc}/\omega_p^n)$, ω_p is the hopping frequency of the charge carriers and n is the dimensionless frequency exponent which lies in the range $0 < n < 1$. The above Eq. is rewritten as,

$$\sigma'(\omega) = \sigma_{dc}\left[1 + \left(\frac{\omega}{\omega_p}\right)^n\right] \tag{3}$$

ω is angular frequency.

The above Eq. is called framework of Almond–West conductivity formalism [29,30]. Many solids, including glasses, polymers, and crystals, show deviation from the Jonscher power law when frequency exceeds ω_p by several orders of magnitude [31–33].

Fig. 6(a) and (b) shows the frequency dependent conductivity in the temperature interval from −100 to 0 °C of $Li_{6.75}La_3Zr_{1.875}Te_{0.125}O_{12}$ and $Li_{6.5}La_3Zr_{1.75}Te_{0.25}O_{12}$, respectively. Two clear dispersion regions were found in the frequency dependent conductivity of $Li_{6.75}La_3Zr_{1.875}Te_{0.125}O_{12}$ and $Li_{6.5}La_3Zr_{1.75}Te_{0.25}O_{12}$ presented as Fig. 6(a) and (b), respectively. The dispersion processes are related to ion transport in the bulk and grain boundaries of the ceramics. The lower frequency part corresponds to the relaxation processes in grain boundaries, and the ionic blocking character of the electrode. The long range conductivity process through the sample is indicated by the presence of a plateau corresponding to the dc conductivity of the Li^+. At high frequency the conductivity displays a dispersive behavior attributed to the relaxation processes in grains as generally observed in ionic conductors. The processes are thermally activated and dispersion regions shift toward higher frequencies as temperature increases.

In Fig. 6(a) and (b) the different symbols represent the experimental ac conductivity data measured at different temperatures and the continuous lines are fitted to Eq. (3). In fitting σ_{dc}, ω_p, and n values are varied to get the best fits, and the parameters obtained by Levenberg–Marquardt nonlinear least-squares fitting are given in Tables 3 and 4 for $Li_{6.75}La_3Zr_{1.875}Te_{0.125}O_{12}$ and $Li_{6.5}La_3Zr_{1.75}Te_{0.25}O_{12}$, respectively. Increase in the σ_{dc} and the ω_p with temperature is due to the increase in the thermally activated drift mobility of ions according to hopping conduction mechanism.

Fig. 7(a) and (b) shows the plots of $\log(\sigma_{dc}T)$ versus $1000/T$ and $\log(\omega_p)$ versus $1000/T$, respectively, for $Li_{6.75}La_3Zr_{1.875}Te_{0.125}O_{12}$ and $Li_{6.5}La_3Zr_{1.75}Te_{0.25}O_{12}$. This temperature dependency is found to obey the Arrhenius Eq.,

$$\sigma_{dc}T = \sigma_0 \exp\left(\frac{-E_\sigma}{k_B T}\right) \tag{4}$$

$$\omega_p = \omega_0 \exp\left(\frac{-E_p}{k_B T}\right) \tag{5}$$

where σ_0 is the dc conductivity pre-exponential factor, E_σ is the dc conductivity activation energy for mobile ions, k_B is the Boltzmann's constant, ω_0 is the pre-exponential of the conductivity relaxation frequency, and E_p is the activation energy for the conductivity relaxation frequency. The activation energy for dc conductivity (E_σ) is found to be close to the activation energy of hopping frequency (E_p).

3.4. *Modulus spectra analysis*

Complex modulus formalism is an important tool to derive information related to charge transport processes. The complex electric modulus (M^*) has been calculated from the complex impedance (Z^*) data using the relation

$$M^*(\omega) = 1/\varepsilon^*(\omega) = i\omega C_0 Z^* = M'(\omega) + iM''(\omega)$$
$$= M_\infty\left[1 - \int_0^\infty \exp(-i\omega t)\left\{\frac{d\phi(t)}{dt}\right\}dt\right] \tag{6}$$

Table 1
Ionic conductivities for the $Li_{6.75}La_3Zr_{1.875}Te_{0.125}O_{12}$ and $Li_{6.5}La_3Zr_{1.75}Te_{0.25}O_{12}$ samples sintered at 750 °C.

S.no.	Nominal composition	Total (bulk + grain boundary) ionic conductivity for the samples sintered at 750 °C					
		−100 °C σ (S cm^{-1})	−50 °C σ (S cm^{-1})	0 °C σ (S cm^{-1})	30 °C σ (S cm^{-1})	50 °C σ (S cm^{-1})	100 °C σ (S cm^{-1})
1.	$Li_{6.75}La_3Zr_{1.875}Te_{0.125}O_{12}$	4.38×10^{-8}	1.63×10^{-7}	7.17×10^{-7}	1.92×10^{-6}	4.10×10^{-6}	6.92×10^{-5}
2.	$Li_{6.5}La_3Zr_{1.75}Te_{0.25}O_{12}$	7.41×10^{-8}	5.98×10^{-7}	7.11×10^{-6}	6.99×10^{-5}	9.76×10^{-5}	1.37×10^{-4}

Table 2
Ionic conductivities and activation energy for $Li_{6.75}La_3Zr_{1.875}Te_{0.125}O_{12}$ and $Li_{6.5}La_3Zr_{1.75}Te_{0.25}O_{12}$ samples sintered at 1100 °C.

S.no.	Nominal composition	Total (bulk + grain boundary) ionic conductivity for the samples sintered at 1100 °C						Activation energy (in the temperature range −100 to 100 °C) E_a (eV)
		−100 °C σ (S cm^{-1})	−50 °C σ (S cm^{-1})	0 °C σ (S cm^{-1})	30 °C σ (S cm^{-1})	50 °C σ (S cm^{-1})	100 °C σ (S cm^{-1})	
1.	$Li_{6.75}La_3Zr_{1.875}Te_{0.125}O_{12}$	6.02×10^{-9}	1.91×10^{-6}	7.28×10^{-5}	3.30×10^{-4}	7.53×10^{-4}	3.52×10^{-3}	0.41
2.	$Li_{6.5}La_3Zr_{1.75}Te_{0.25}O_{12}$	9.37×10^{-9}	4.09×10^{-6}	2.03×10^{-4}	1.02×10^{-3}	2.42×10^{-3}	1.24×10^{-2}	0.38

where $\varepsilon^*(\omega)$ is the complex permittivity, C_0 is the geometrical capacitance $= \varepsilon_0 A/t$ (ε_0 = permittivity of free space, A = area of the electrode and t = thickness), M' = real part of the electric modulus, M'' = imaginary part of the electric modulus, $M_\infty = 1/\varepsilon_\infty$, ($\varepsilon_\infty$ is the high frequency asymptotic value of the real part of the dielectric permittivity) and the relaxation function $\varphi(t)$ gives the time evolution of the electric field within the material.

Fig. 8(a) and (b) shows the imaginary part of the electric modulus (M'') with log(f) of $Li_{6.75}La_3Zr_{1.875}Te_{0.125}O_{12}$ and $Li_{6.5}La_3Zr_{1.75}Te_{0.25}O_{12}$ measured at different temperatures in the temperature range from −100 to 0 °C. The frequency dependence of

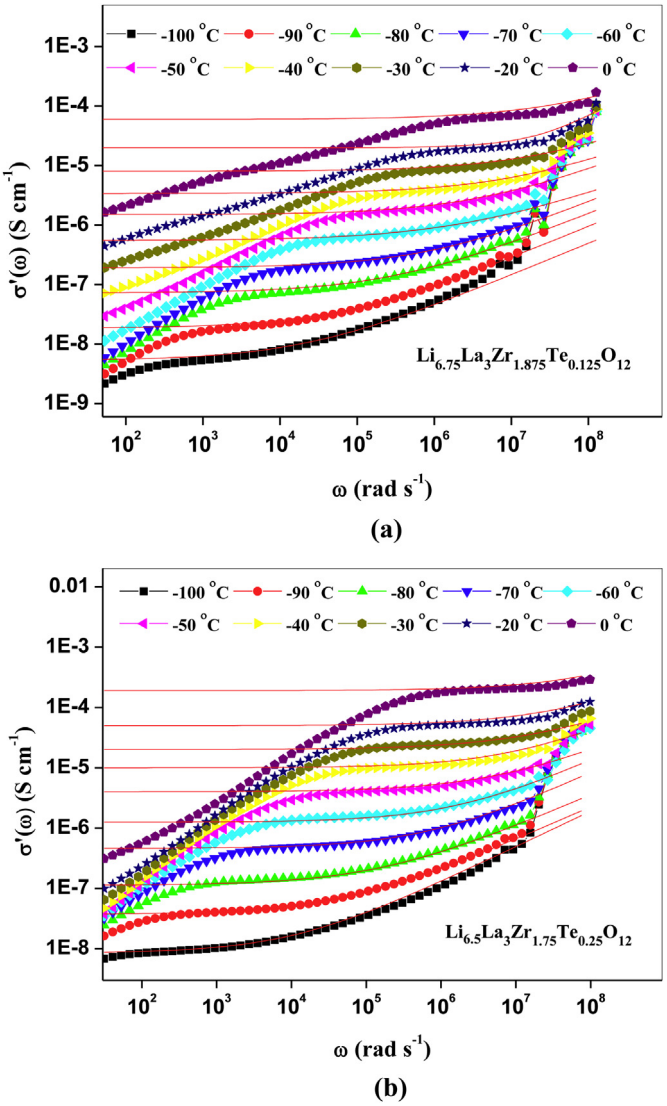

Fig. 6. Frequency dependent conductivity measured in the temperature interval from −100 to 0 °C of (a) $Li_{6.75}La_3Zr_{1.875}Te_{0.125}O_{12}$ and (b) $Li_{6.5}La_3Zr_{1.75}Te_{0.25}O_{12}$. The solid lines are best fit to the Almond–West conductivity formalism [29].

imaginary part of the electric modulus (M'') measured at different temperatures (−100 to 0 °C) of $Li_{6.75}La_3Zr_{1.875}Te_{0.125}O_{12}$ and $Li_{6.5}La_3Zr_{1.75}Te_{0.25}O_{12}$ shown in Fig. 8(a) and (b) indicated visibly resolved peaks at unique frequency. The appearance of peak in modulus spectrum provides a clear signal of conductivity relaxation. The low frequency wing below peak maximum (M_{max}'') represents the range in which the charge carriers are mobile at long distances; i.e., ions can perform successful hopping from one site to the neighboring site. On the other hand, at frequencies above peak maximum, the carriers are confined to potential wells and are mobile at short distances.

The position of the peaks (M_{max}'') in Fig. 8(a) and (b) shifts towards higher frequencies as temperature is increased. This behavior suggests that the relaxation rate for this process increases with increasing temperature in which hopping mechanism of charge carriers dominates intrinsically. The peak frequency f_m represents the most probable conductivity relaxation frequency from the relation $f_m\tau_m = 1$, where τ_m is the characteristic relaxation time represents the time scale of the transition from the long-range to short-range mobility.

A better information on the bulk conduction properties may be obtained from Arrhenius plots of frequency (f_m) at the modulus peak maximum M''_{max} [34]. The activation energy (E_a) was calculated from,

$$f_m T = f_0 \exp\left(\frac{-E_a}{k_B T}\right) \quad (7)$$

where f_0 is the pre-exponential parameter of the relaxation frequency. The Arrhenius plots of log(f_mT) versus 1000/T obtained from the temperature range −100 to 0 °C for $Li_{6.75}La_3Zr_{1.875}Te_{0.125}O_{12}$ and $Li_{6.5}La_3Zr_{1.75}Te_{0.25}O_{12}$ are shown in Fig. 9. The similarity in the activation energy derived from the slope of log(f_mT) versus 1000/T and log(σT) versus 1000/T suggests the long-range translational motion of Li^+.

The modulus scaling behavior gives an insight into the dielectric process occurring inside the material. We have scaled M'' by M_{max}'' and each frequency by f_{max}, where f_{max} corresponds to the frequencies of the peak positions in M_{max}'' versus log f plots. Fig. 10(a) and (b) show the normalized imaginary part of the modulus (M''/M_{max}'') versus normalized log(f/f_{max}) measured at various

Table 3
Parameters derived from the fits of ac conductivity measurements for $Li_{6.75}La_3Zr_{1.875}Te_{0.125}O_{12}$.

Temp (°C)	σ_{dc} (S cm^{-1})	A (S cm^{-1} rad^{-n})	n	ω_p (rad s^{-1})
−100	6.22×10^{-09}	2.37×10^{-11}	0.54	3.02×10^{4}
−90	1.65×10^{-08}	4.51×10^{-11}	0.53	6.86×10^{4}
−80	7.25×10^{-08}	8.72×10^{-11}	0.53	3.23×10^{5}
−70	1.92×10^{-07}	1.12×10^{-10}	0.54	9.79×10^{5}
−60	8.65×10^{-07}	5.67×10^{-10}	0.49	3.13×10^{6}
−50	2.10×10^{-06}	6.00×10^{-10}	0.52	6.54×10^{6}
−40	4.20×10^{-06}	8.29×10^{-10}	0.51	1.84×10^{7}
−30	9.04×10^{-06}	1.06×10^{-09}	0.52	3.62×10^{7}
−20	2.00×10^{-05}	2.08×10^{-09}	0.51	6.48×10^{7}
0	8.20×10^{-05}	4.88×10^{-09}	0.49	4.19×10^{8}

Table 4
Parameters derived from the fits of ac conductivity measurements for $Li_{6.5}La_3Zr_{1.75}Te_{0.25}O_{12}$.

Temp (°C)	σ_{dc} (S cm^{-1})	A (S cm^{-1} rad^{-n})	n	ω_p (rad s^{-1})
−100	9.99×10^{-09}	3.44×10^{-11}	0.54	3.64×10^{4}
−90	7.50×10^{-08}	9.42×10^{-11}	0.57	1.23×10^{5}
−80	2.00×10^{-07}	1.82×10^{-10}	0.55	3.38×10^{5}
−70	5.92×10^{-07}	2.92×10^{-10}	0.55	1.03×10^{6}
−60	1.55×10^{-06}	3.12×10^{-10}	0.58	2.36×10^{6}
−50	4.51×10^{-06}	8.92×10^{-10}	0.55	5.43×10^{6}
−40	1.01×10^{-05}	1.08×10^{-09}	0.56	1.23×10^{7}
−30	2.00×10^{-05}	3.95×10^{-09}	0.50	2.56×10^{7}
−20	4.00×10^{-05}	4.99×10^{-09}	0.50	6.43×10^{7}
0	2.10×10^{-04}	9.99×10^{-09}	0.51	2.99×10^{8}

temperatures of $Li_{6.75}La_3Zr_{1.875}Te_{0.125}O_{12}$ and $Li_{6.5}La_3Zr_{1.75}Te_{0.25}O_{12}$, respectively.

The low frequency side of the peak in M''/M_{max}'' versus $\log(f/f_{max})$ curve represents the range of frequencies in which the charge carriers can cover a longer distance by successfully hopping from one site to another site. The high frequency side of M''/M''_{max} versus $\log(f/f_{max})$ curve represents the range of frequencies in which the

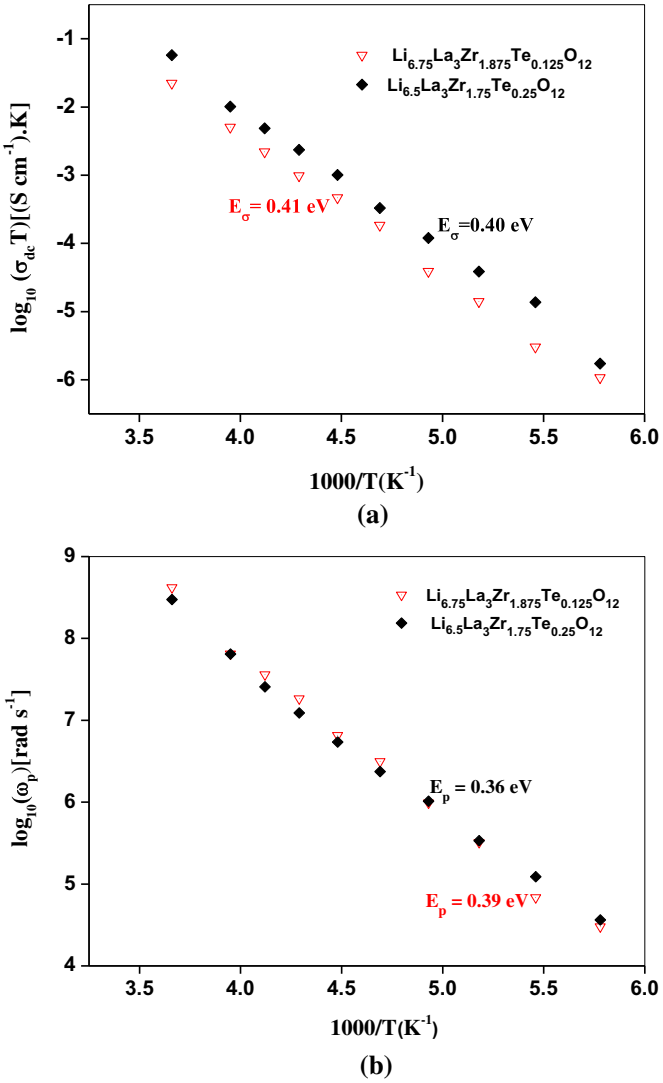

Fig. 7. Arrhenius plot (a) $\log_{10}(\sigma_{dc}T)$ versus $1000/T$ and (b) $\log_{10}(\omega_p)$ versus $1000/T$ of $Li_{6.75}La_3Zr_{1.875}Te_{0.125}O_{12}$ and $Li_{6.5}La_3Zr_{1.75}Te_{0.25}O_{12}$.

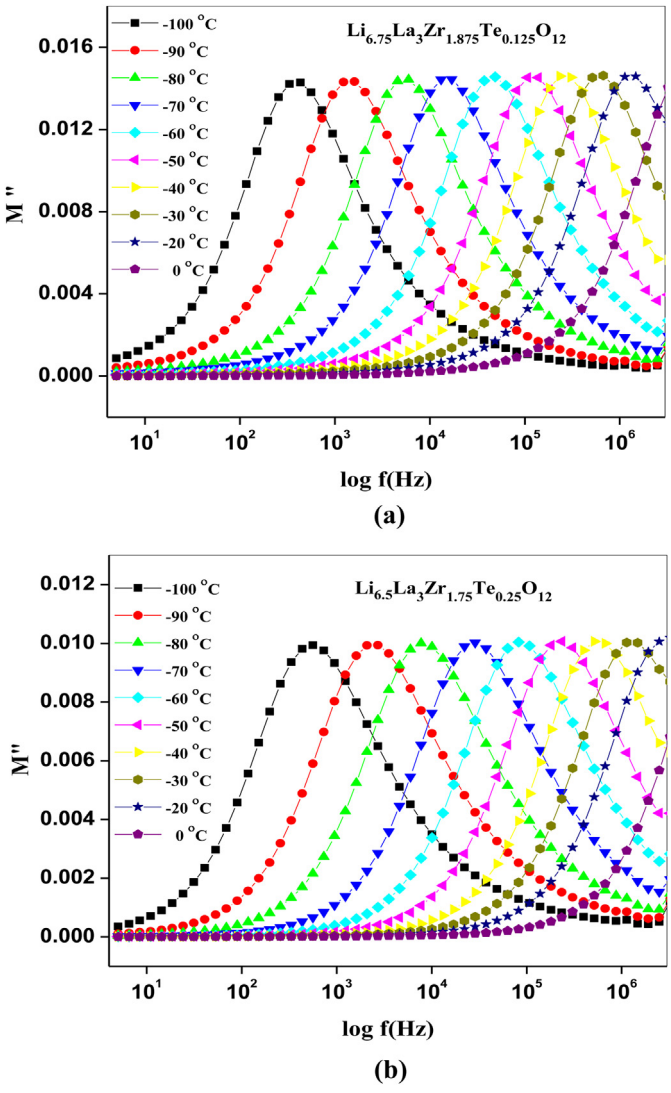

Fig. 8. Plot of imaginary part of modulus (M'') versus $\log(f)$ of (a) $Li_{6.75}La_3Zr_{1.875}Te_{0.125}O_{12}$ and (b) $Li_{6.5}La_3Zr_{1.75}Te_{0.25}O_{12}$.

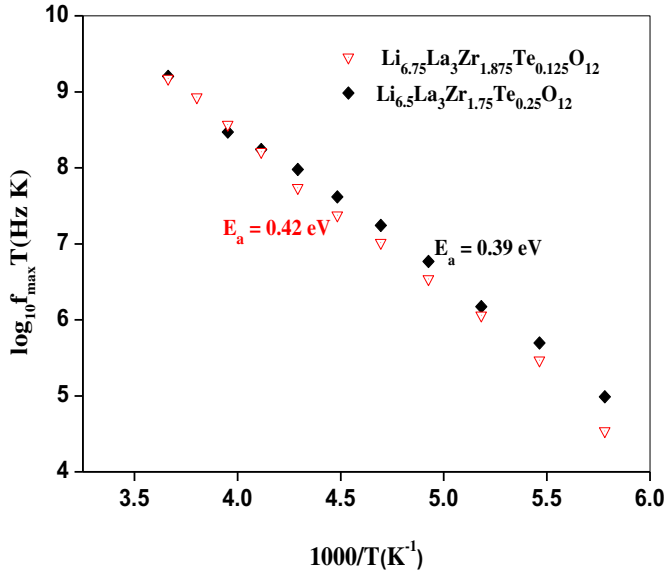

Fig. 9. Arrhenius plots of $\log_{10}(f_{max}T)$ versus $1000/T$ in the temperature interval from −100 to 0 °C of $Li_{6.75}La_3Zr_{1.875}Te_{0.125}O_{12}$ and $Li_{6.5}La_3Zr_{1.75}Te_{0.25}O_{12}$.

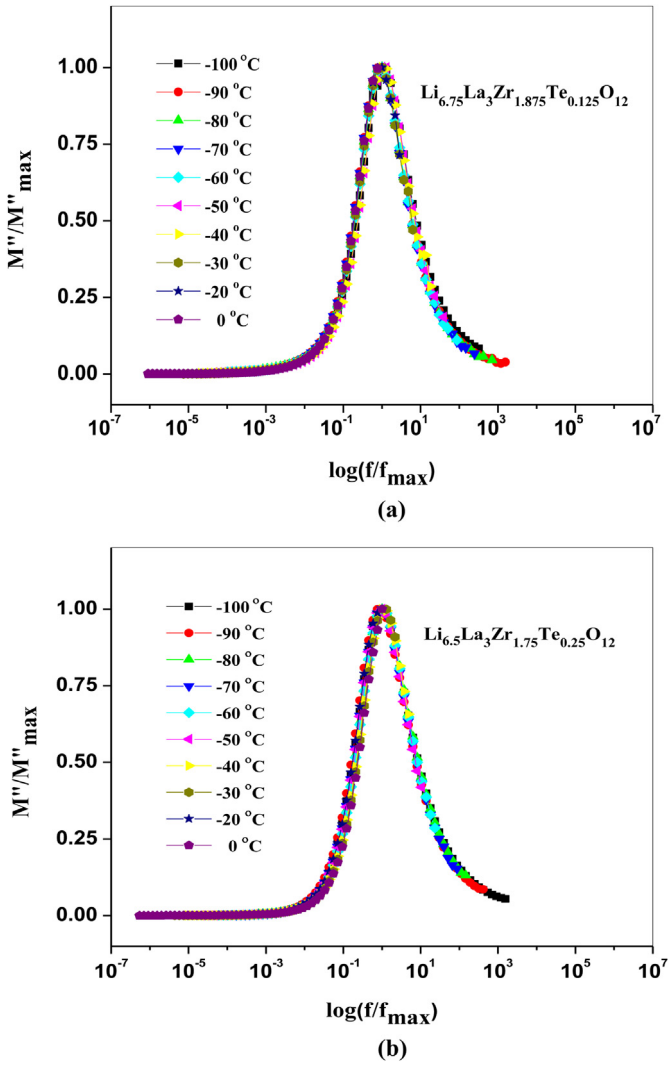

Fig. 10. Modulus scaling behavior of (a) $Li_{6.75}La_3Zr_{1.875}Te_{0.125}O_{12}$ and (b) $Li_{6.5}La_3Zr_{1.75}Te_{0.25}O_{12}$.

charge carriers are spatially confined to their potential wells, and therefore can make only localized motions inside the well. The region where the peak occurs is an indication of the transition from the long-range to the short-range mobility with increase in frequency [35]. The overlapping of all the peaks of different temperatures indicates that all dynamic processes occurring at different time scales exhibit the same activation energy and that the distribution of relaxation process is independent of temperature [36].

The full width at half maximum (FWHM) value derived from the master modulus curve of $Li_{6.75}La_3Zr_{1.875}Te_{0.125}O_{12}$ and $Li_{6.5}La_3Zr_{1.75}Te_{0.25}O_{12}$ were found to be 1.574 and 1.531 decade, respectively. The FWHM for the master modulus curve of the $Li_{6.75}La_3Zr_{1.875}Te_{0.125}O_{12}$ and $Li_{6.5}La_3Zr_{1.75}Te_{0.25}O_{12}$ are wider than the width of a typical Debye peak (1.14 decade) suggesting the presence of non-Debye type conductivity relaxation phenomena.

4. Conclusion

Te substituted $Li_{6.75}La_3Zr_{1.875}Te_{0.125}O_{12}$ and $Li_{6.5}La_3Zr_{1.75}Te_{0.25}O_{12}$ lithium garnets were successfully synthesized by conventional solid state method. The PXRD indicated that the selected compositional range was found to crystallize in the garnet like structure with cubic symmetry relatively at lower sintering temperature around 750 °C. The ac conductivity of $Li_{6.75}La_3Zr_{1.875}Te_{0.125}O_{12}$ and $Li_{6.5}La_3Zr_{1.75}Te_{0.25}O_{12}$ has been investigated over a wide temperature range. Among the investigated compounds $Li_{6.5}La_3Zr_{1.75}Te_{0.25}O_{12}$ exhibits a maximum total ionic conductivity of 1.02×10^{-3} S cm^{-1} at 30 °C. The FWHM for master modulus curve of $Li_{6.5}La_3Zr_{1.75}Te_{0.25}O_{12}$ was found to be least among the investigated lithium garnets. The overlap of the normalized modulus spectra obtained for different temperatures indicates that the distribution of relaxation process is independent of temperature. The present studies support the earlier prediction of optimum Li^+ concentration required for maximum room temperature Li^+ conductivity in $Li_{7-x}La_3Zr_{2-x}M_xO_{12}$ is around $x = 0.4 \pm 0.1$. The present studies revealed the stabilization of the cubic garnet phase relatively at lower sintering temperature along with an enhancement in Li^+ conductivity with lithium content lesser than 7 by suitable doping in $Li_7La_3Zr_2O_{12}$. Further work on the electrochemical stability of this high Li^+ conductive Te substituted LLZ is under way.

Acknowledgments

R.M. thanks the DRDO, New Delhi, India for the financial support (No: ERIP/ER/0804415/M/01/1183/4.11.2009). Authors thank CIF Pondicherry University, India for extending the instrumentation facilities.

References

[1] V. Thangadurai, H. Kaack, W. Weppner, J. Am. Ceram. Soc. 86 (2003) 437.
[2] V. Thangadurai, W. Weppner, J. Am. Ceram. Soc. 88 (2005) 411.
[3] V. Thangadurai, W. Weppner, Adv. Funct. Mater. 15 (2005) 107.
[4] V. Thangadurai, W. Weppner, J. Solid State Chem. 179 (2006) 974.
[5] R. Murugan, V. Thangadurai, W. Weppner, Angew. Chem. Int. Ed. 46 (2007) 7778.
[6] R. Murugan, W. Weppner, P. Schmid-Beurmann, V. Thangadurai, Mater. Sci. Eng. B 143 (2007) 14.
[7] R. Murugan, V. Thangadurai, W. Weppner, Ionics 13 (2007) 195.
[8] R. Murugan, W. Weppner, P. Schmid-Beurmann, V. Thangadurai, Mater. Res. Bull. 43 (2008) 2579.
[9] R. Murugan, V. Thangadurai, W. Weppner, Appl. Phys. A 91 (2008) 615.
[10] T. Zaib, M. Ortnet, R. Murugan, W. Weppner, Ionics 16 (2009) 855.
[11] J. Awaka, N. Kijima, H. Hayakawa, J. Akimoto, J. Solid State Chem. 182 (2009) 2046.
[12] M. Kotobuki, K. Kanamura, Y. Sato, T. Yoshida, J. Power Sources 196 (2011) 7750.
[13] S. Kumazaki, Y. Iriyama, K.H. Kim, R. Murugan, K. Tanabe, K. Yamamoto, T. Hirayama, Z. Ogumi, Electrochem. Commun. 13 (2011) 509.
[14] C.A. Geiger, E. Alekseev, B. Lazic, M. Fisch, T. Armbruster, R. Langner, M. Fechtelkord, N. Kim, T. Pettke, W. Weppner, Inorg. Chem. 50 (2011) 1089.
[15] A. Duevel, A. Kuhn, L. Robben, M. Wilkening, P. Heitjans, J. Phys. Chem. C 116 (2012) 15192.
[16] N. Janani, S. Ramakumar, R. Murugan, Fast lithium ion conduction in zirconium containing garnet structured ceramic electrolyte, in: International Ceramic Congress (ICC3), Osaka, Japan, Nov., 2010, p. S9A.
[17] Y. Li, C.A. Wang, H. Xie, J. Cheng, J.B. Goodenough, Electrochem. Commun. 13 (2011) 1289.
[18] A. Logéat, T. Köhler, U. Eisele, B. Stiaszny, A. Harzer, M. Tovar, A. Senyshyn, H. Ehrenberg, B. Kozinsky, Solid State Ionics 206 (2012) 33.
[19] Y. Wang, W. Lai, Electrochem. Solid-State Lett. 15 (2012) A68.
[20] S. Ohta, T. Kobayashi, J. Seki, T. Asaoka, J. Power Sources 202 (2012) 332.
[21] N. Sumaletha, F. Ramezanipour, V. Thangadurai, J. Phys. Chem. C 116 (2012) 20154.
[22] J.L. Allen, J. Wolfenstine, E. Rangasamy, J. Sakamoto, J. Power Sources 206 (2012) 315.
[23] M. Huang, A. Dumon, C.W. Nan, Electrochem. Commun. 21 (2012) 62.
[24] R. Murugan, S. Ramakumar, N. Janani, Electrochem. Commun. 13 (2011) 1373.
[25] R.D. Shannon, Acta Crystallogr. A 32 (1976) 751.
[26] Y. Li, J.T. Han, C.A. Wang, H. Xie, J.B. Goodenough, J. Mater. Chem. 22 (2012) 15357.
[27] G. Asha, R. Murugan, M. Parans Paranthaman, Z. Bi, C.A. Bridges, M. Nakanishi, A.P. Sokolov, K.S. Han, E.W. Hagaman, H. Xie, C.B. Mullins, J.B. Goodenough, J. Power Sources 209 (2012) 184.

[28] A.K. Jonscher, Dielectric Relaxation in Solids, Chelsea Dielectric Press, London, 1983.
[29] D.P. Almond, G.K. Duncan, A.R. West, Solid State Ionics 9-10 (1983) 277.
[30] A. Pan, A. Ghosh, Phys. Rev. B 60 (1999) 3224.
[31] A.R. Long, Adv. Phys. 31 (1982) 553.
[32] W.K. Lee, J.F. Liu, A.S. Nowick, Phys. Rev. Lett. 67 (1991) 1559.
[33] A.S. Nowik, B.S. Lim, A.V. Vagsleyb, J. Non-Cryst. Solids 1243 (1994) 172.
[34] E.R. Losilla, M.A.G. Aranda, S. Bruque, M. Paris, J. Sanz, A.R. West, Chem. Mater. 10 (1998) 665.
[35] P.S. Das, P.K. Chakraborty, B. Behera, R.N.P. Choudhary, Phys. B 395 (2007) 98.
[36] S. Saha, T.P. Sinha, Phys. Rev. B 65 (2002) 134103.